Microenvironment Modulation Hot Paper

How to cite: *Angew. Chem. Int. Ed.* **2021**, *60*, 16372–16376
International Edition: doi.org/10.1002/anie.202104219
German Edition: doi.org/10.1002/ange.202104219

Interfacial Microenvironment Modulation Boosting Electron Transfer between Metal Nanoparticles and MOFs for Enhanced Photocatalysis

*Mingliang Xu, Dandan Li, Kang Sun, Long Jiao, Chenfan Xie, Chunmei Ding, and Hai-Long Jiang**

Abstract: *Interfacial electron transfer between cocatalyst and photosensitizer is key in heterogeneous photocatalysis, yet the underlying mechanism remains subtle and unclear. Surfactant coated on the metal cocatalysts, greatly modulating the microenvironment of catalytic sites, is largely ignored. Herein, a series of Pt co-catalysts with modulated microenvironments, including polyvinylpyrrolidone (PVP) capped Pt nanoparticles (denoted as Pt_{PVP}), Pt with partially removed PVP (Pt_{rPVP}), and clean Pt without PVP (Pt), were encapsulated into a metal–organic framework (MOF), UiO-66-NH_2, to afford Pt_{PVP}@UiO-66-NH_2, Pt_{rPVP}@UiO-66-NH_2, and Pt@UiO-66-NH_2, respectively, for photocatalytic hydrogen production. The PVP appears to have a negative influence on the interfacial electron transfer between Pt and the MOF. Compared with Pt_{PVP}@UiO-66-NH_2, the removal of interfacial PVP improves the sluggish kinetics of electron transfer, boosting photocatalytic hydrogen production.*

Photocatalytic water splitting to hydrogen driven by solar energy is deemed to be a green strategy to address global energy and environmental issues.[1] However, toward efficient photocatalytic hydrogen production by water splitting, there are currently significant challenges, for example, the weak light harvesting capability, the high recombination rate of photo-generated electron-hole (e-h) pairs, and insufficient reaction sites, etc.[2] Amongst them, the fast recombination of charge carriers is recognized to be one of the decisive factors.[2b] To tackle this hurdle, the introduction of co-catalysts has been widely accepted as an effective way to suppress the recombination of photo-generated carriers.[1,3] Especially, Pt nanoparticles (NPs), with a large work function and low H_2 evolution overpotential, have been identified as the most effective cocatalyst for H_2 production.[4]

Given that Pt NPs are catalytic sites, their sizes and morphology have great influences on the resulting performance, and the smaller Pt NPs usually give higher activity.[5] To control the Pt size and morphology, surfactant (e.g. PVP) is always adopted and remained at the interface between Pt and photosensitizer (support), which would create a particular microenvironment around Pt NPs.[5a,6] Therefore, regulating the coverage of interfacial surfactant, which can modulate the microenvironment surrounding catalytic sites, should be an effective strategy to improve the interfacial electron transfer. Unfortunately, the related investigation is largely overlooked. In fact, upon removing the interfacial PVP, Pt NPs on common supports (as photosensitizers) would be readily aggregated, making it a significant challenge to obtain direct control data with or without PVP. In this context, comparing to traditional supports, crystalline porous materials have been widely adopted as supports to stabilize and disperse metal NPs, owing to the effect of pore confinement.[7] Therefore, crystalline porous materials would be suitable and desirable to encapsulate Pt NPs and avoid their agglomeration, even without PVP protection.

As promising crystalline porous materials, metal–organic frameworks (MOFs), constructed by metal ions/clusters and organic linkers via coordination bonds, are suitable hosts to encapsulate tiny metal NPs.[8,9,12] The Pt sites can be well stabilized and accessible after being encapsulated into MOFs, thanks to the porous structures. Furthermore, MOFs have been well accepted as photosensitizers,[10] with Pt as a co-catalyst to improve the charge separation.[11] Therefore, the encapsulation of Pt NPs into MOFs would be an ideal model to investigate the surfactant influence on interfacial electron transfer and corresponding activity in photocatalysis.

With this in mind, a representative MOF, UiO-66-NH_2 ($Zr_6O_4(OH)_4(BDC\text{-}NH_2)_6$, BDC-$NH_2$ = 2-amino-1,4-benzenedicarboxylic acid), is chosen as it possesses regular morphology, high stability, and visible-light responsive feature, suitable for stabilizing dispersed Pt NPs.[6b,9c] With this MOF as a photosensitizer and support, PVP capped Pt NPs (denoted as Pt_{PVP}), Pt with partially removed PVP (Pt_{rPVP}), and clean Pt without PVP (Pt), with similar particle sizes (ca. 2.5 nm) and loadings (ca. 2.5 wt%), are incorporated, affording Pt_{PVP}@UiO-66-NH_2, Pt_{rPVP}@UiO-66-NH_2, and Pt@UiO-66-NH_2 nanocomposites, respectively (Scheme 1). Remarkably, the gradual removal of interfacial PVP gives rise to increased electrical conductivity and benefits the electron transfer between the MOF and Pt sites. As a result, Pt@UiO-66-NH_2 greatly suppresses the electron-hole recombination,

[*] M. Xu, K. Sun, Dr. L. Jiao, C. Xie, Prof. Dr. H.-L. Jiang
Hefei National Laboratory for Physical Sciences at the Microscale, CAS Key Laboratory of Soft Matter Chemistry, Department of Chemistry, University of Science and Technology of China
Hefei, Anhui 230026 (P. R. China)
E-mail: jianglab@ustc.edu.cn
Homepage: http://staff.ustc.edu.cn/~jianglab/
Dr. D. Li
Institute of Physical Science and Information Technology
Anhui University, Hefei, Anhui 230601 (P. R. China)
Dr. C. Ding
Dalian National Laboratory for Clean Energy, State Key Laboratory of Catalysis, Dalian Institute of Chemical Physics
Chinese Academy of Sciences
Dalian, Liaoning 116023 (P. R. China)
Supporting information and the ORCID identification number(s) for the author(s) of this article can be found under: https://doi.org/10.1002/anie.202104219.

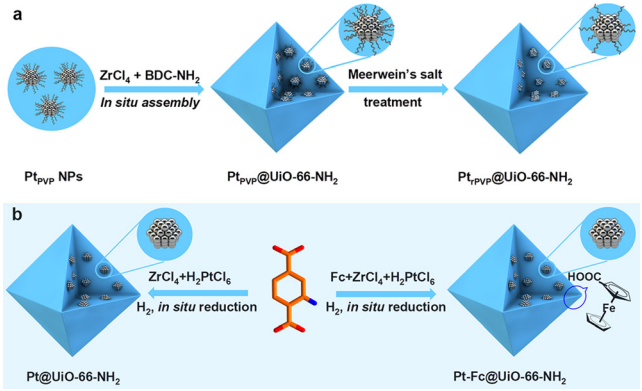

Scheme 1. Illustration of the synthetic strategies for different photocatalysts: a) Pt_{PVP}@UiO-66-NH_2 and Pt_{rPVP}@UiO-66-NH_2; b) Pt@UiO-66-NH_2, and Pt-Fc@UiO-66-NH_2.

and hence brings about its much-enhanced activity compared to Pt_{PVP}@UiO-66-NH_2 and Pt_{rPVP}@UiO-66-NH_2. Furthermore, introducing Ferrocene carboxylic acid (Fc) as the electron mediator into Pt@UiO-66-NH_2 further improves the charge separation, and the resultant Pt-Fc@UiO-66-NH_2 presents the best photocatalytic performance. As far as we know, this is the first report on investigating the influence of interfacial microenvironment (surfactant) between photosensitizer and cocatalyst in photocatalysis.

The Pt_{PVP} NPs with uniform sizes of ca. 2.5 nm are synthesized based on the documented method (Figure S1 in the Supporting Information).[6b] The Pt_{PVP} NPs are redispersed in DMF with $ZrCl_4$ and BDC-NH_2 to afford Pt_{PVP}@UiO-66-NH_2 under solvothermal conditions. Powder X-ray diffraction (XRD) patterns show the well-retained MOF structure in the Pt_{PVP}@UiO-66-NH_2 nanocomposite (Figure S2). After being treated by the Meerwein's salt solution with different time lengths, PVP in Pt_{PVP}@UiO-66-NH_2 can be partially removed, yielding Pt_{rPVP}@UiO-66-NH_2 nanocomposite (the optimized and default treatment time is 9 h).[12] The ^{1}H-NMR signals manifest the existence of PVP in Meerwein's salt solution after Pt_{PVP}@UiO-66-NH_2 is soaked, supporting the removal of PVP from Pt_{PVP} NPs (Figure S3). The diffuse reflectance infrared Fourier transform (DRIFT) spectra of CO adsorption indicate that Pt_{PVP}@UiO-66-NH_2 and Pt_{rPVP}@UiO-66-NH_2 present distinctly different adsorption behaviors, which are in accordance with the results of Pt_{PVP} and surface-clean Pt supported on the inert SiO_2 substrate, demonstrating the above results (Figure S4). Powder XRD patterns indicate that the retained MOF structure after the treatment in Meerwein's salt solution up to 9–10 hours (Figure S5), and the removed PVP amount was evaluated (Table S1). To guarantee the absolute absence of PVP, Pt NPs with clean surface are incorporated into UiO-66-NH_2, during which the Pt precursors are dispersed in the precursor solution of UiO-66-NH_2 and in situ reduced in H_2 atmosphere to afford Pt@UiO-66-NH_2. Powder XRD patterns demonstrate the intact MOF crystallinity in Pt@UiO-66-NH_2 (Figure S2). Nitrogen sorption isotherms of UiO-66-NH_2, Pt_{PVP}@UiO-66-NH_2, Pt_{rPVP}@UiO-66-NH_2, and Pt@UiO-66-NH_2 exhibit the typical type-I microporous isotherms, with the BET surface area of 993, 672, 808, and 729 $m^2 g^{-1}$, respectively (Figure S6). The reduced surface areas of Pt_{PVP}@UiO-66-NH_2, Pt_{rPVP}@UiO-66-NH_2, and Pt@UiO-66-NH_2 than UiO-66-NH_2 are reasonable and attributed to the Pt incorporation. The slightly higher surface area of Pt_{rPVP}@UiO-66-NH_2 than Pt_{PVP}@UiO-66-NH_2 supports that PVP is removed in the former sample.

Scanning electron microscopy (SEM) observation shows that all the nanocomposites are ca. 200 nm and in an octahedral shape which is similar to that of the parent MOF (Figure S7). Transmission electron microscopy (TEM) images suggest that the incorporated Pt_{PVP}, Pt_{rPVP}, and Pt NPs are well-dispersed inside MOFs with comparable sizes of ca. 2.5 nm. To our delight, the sizes and shapes of both UiO-66-NH_2, and Pt NPs in Pt_{PVP}@UiO-66-NH_2 are almost maintained after being treated in Meerwein's salt solution (Figure 1 and S8). The Pt loading amounts in these nanocomposites are similar (ca. 2.5 wt%; Table S2). UV/Vis diffuse reflectance spectra of all these samples well inherit

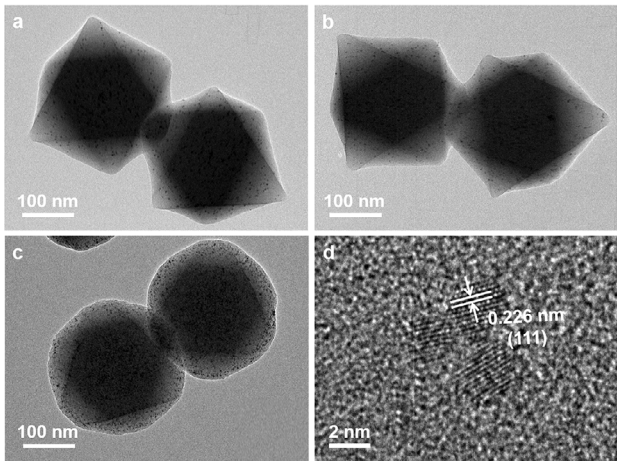

Figure 1. TEM images of a) Pt_{PVP}@UiO-66-NH_2, b) Pt_{rPVP}@UiO-66-NH_2, and c) Pt@UiO-66-NH_2. d) High-resolution TEM image for the Pt NPs in Pt@UiO-66-NH_2. The lattice fringe with a spacing of 0.226 nm is indexed to the Pt (111) plane.[13]

the MOF feature and give roughly the same profiles in the range of 200–800 nm, indicating their comparable light harvesting capability mainly caused by the MOF (Figure 2a). The band structure of UiO-66-NH_2 shows that it is suitable for photocatalytic H_2 production (Figure S9).

To examine the charge separation efficiency, electrochemical impedance spectroscopy (EIS), photocurrent response, and photoluminescence (PL) emission spectroscopy have been examined. The radius of Nyquist plots follows a trend of UiO-66-NH_2 > Pt_{PVP}@UiO-66-NH_2 > Pt_{rPVP}@UiO-66-NH_2 > Pt@UiO-66-NH_2 (Figure 2b), revealing that the existence of PVP disfavors the electrical conductivity and causing charge transfer resistance. This argument is supported by the photocurrent results, where the intensity order follows UiO-66-NH_2 < Pt_{PVP}@UiO-66-NH_2 < Pt_{rPVP}@UiO-66-NH_2 < Pt@UiO-66-NH_2 (Figure 2c). Photoluminescence (PL) emission spectroscopy, which offers important information for charge transfer and recombination, has further provided

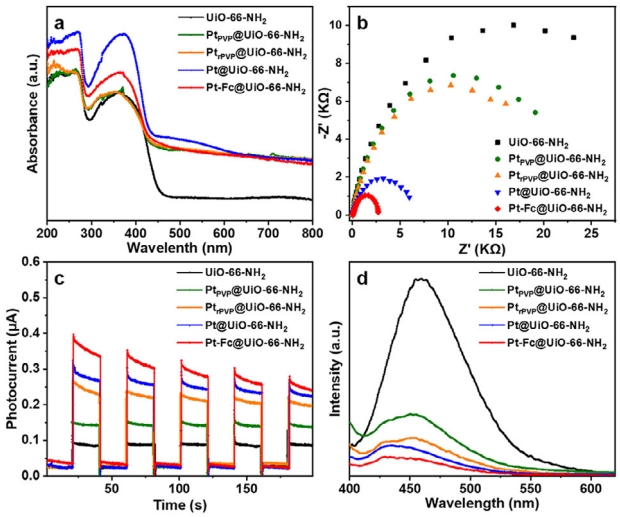

Figure 2. a) UV/Vis diffuse reflectance spectra, b) EIS Nyquist plots, c) photocurrent responses, d) PL emission spectra (excited at 380 nm) for UiO-66-NH_2, Pt_{PVP}@UiO-66-NH_2, Pt_{rPVP}@UiO-66-NH_2, Pt@UiO-66-NH_2, and Pt-Fc@UiO-66-NH_2.

supportive results (Figure 2d). Under 380 nm excitation, the steady-state PL emission for UiO-66-NH_2 at ca. 455 nm arises from direct e-h recombination at room temperature. The emission intensity is significantly weakened when Pt NPs are incorporated and is further suppressed when the interfacial PVP is removed. These results corroborate each other that the recombination of photo-generated e-h pairs is suppressed and electron transfer is promoted by PVP removal.

To further improve electron transfer, Ferrocene carboxylic acid (Fc) serving as the electron mediator is introduced to the synthetic system, yielding Pt-Fc@UiO-66-NH_2 (Scheme 1b). The Fc remains intact after being introduced into Pt@UiO-66-NH_2 as evidenced by ^{1}H NMR spectra (Figure S10) and the retained MOF structure in Pt-Fc@UiO-66-NH_2 can be supported by powder XRD pattern (Figure S2). X-ray photoelectron spectroscopy (XPS) spectra show the higher binding energy of Zr $3d_{5/2}$ after introducing Fc into Pt@UiO-66-NH_2, revealing the interaction between Fc and Zr-oxo clusters (Figure S11).[14] When Fc is replaced by Ferrocene, only very few Ferrocene (Fe/Zr = 0.0023) can be introduced, supporting the coordination interaction between Zr-oxo and Fc. Elemental mapping for a random slice of Pt-Fc@UiO-66-NH_2 particles show the even dispersion of Fc in the slice (Figure S12). All these results manifest that Fc is introduced into the MOF and coordinated with Zr-oxo clusters. Moreover, the addition of Fc does not affect the Pt sizes and overall morphology of the catalyst (Figure S8 and S13). As expected, upon introducing the electron mediator of Fc, electron transfer efficiency is further improved. The Pt-Fc@UiO-66-NH_2 displays the smallest radius, the strongest photocurrent response, and the weakest PL emission intensity among all investigated nanocomposites (Figure 2b–d). The distinctly different optical and electrochemical properties among the nanocomposites noted above imply the possibly best photocatalytic activity of Pt-Fc@UiO-66-NH_2.

Encouraged by the above results, we set out to investigate the photocatalytic H_2 production of the above photocatalysts under visible light irradiation. As expected, Pt_{rPVP}@UiO-66-NH_2 presents an obviously higher H_2 production rate than Pt_{PVP}@UiO-66-NH_2 (242.7 μmol g^{-1} h^{-1}), and the activity gradually increases along with the extended soaking time of Pt_{PVP}@UiO-66-NH_2 in Meerwein's salt solution. The best activity (375.9 μmol g^{-1} h^{-1}) of Pt_{rPVP}@UiO-66-NH_2 can be observed when the soaking time reaches 9 h (Figure S14). Significantly, despite almost all similar parameters except for the altered microenvironment (PVP removal) surrounding Pt sites, Pt@UiO-66-NH_2 exhibits an even higher H_2 production rate (400.7 μmol g^{-1} h^{-1}) (Figure 3a), unambiguously illustrating that the presence of interfacial PVP is unfavorable to the activity. As expected, upon boosting electron transfer, Pt-Fc@UiO-66-NH_2 has the optimized amount of Fc possesses the highest photocatalytic H_2 production rate of 514.8 μmol g^{-1} h^{-1} (Figure 3a, Table S3). Moreover, the activity increase is almost linear along with suitably increased amount of Pt-Fc@UiO-66-NH_2 catalyst in the reaction system (Figure S15). As a control, Fc@UiO-66-NH_2 cannot generate H_2, hinting Pt is active site. In sharp contrast, when Fc is directly decorated on the external surface of Pt@UiO-66-NH_2, the obtained Pt@UiO-66-NH_2/Fc could well retain MOF structure (Figure S16), and presents much reduced H_2 production rate (102.6 μmol g^{-1} h^{-1}), which might be ascribed to the steric hindrance of Fc preventing its encapsulation within UiO-66-NH_2 and the electron transfer from the MOF mainly to Fc instead of Pt.[15] The role of Fc in the photocatalytic H_2 production reaction is further decoded by in situ electron spin resonance (ESR). Both ESR and XPS results indicate that the Fe species in Fc is partially oxidized upon incorporating Fc to afford Pt-Fc@UiO-66-NH_2 (Figure S17 and S18).

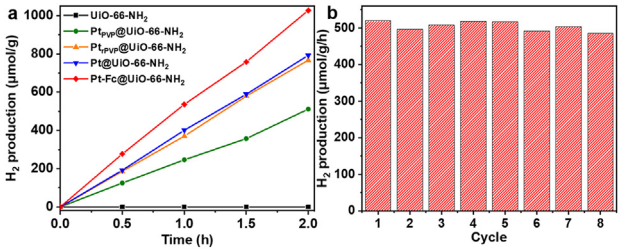

Figure 3. a) Photocatalytic hydrogen production of UiO-66-NH_2, Pt_{PVP}@UiO-66-NH_2, Pt_{rPVP}@UiO-66-NH_2, Pt@UiO-66-NH_2, and Pt-Fc@UiO-66-NH_2 along with time. b) Recycling performance of Pt-Fc@UiO-66-NH_2.

Further recycling experiments for Pt-Fc@UiO-66-NH_2 suggest that no noticeable degradation can be observed in the hydrogen production rate during the eight consecutive catalytic runs (Figure 3b), indicating its high stability. The structural integrity and crystallinity, as well as Pt size and dispersion of Pt-Fc@UiO-66-NH_2 are maintained after the reaction, as indicated by powder XRD pattern and TEM data (Figure S19), thanks to the great confinement effect by the stable MOF structure.

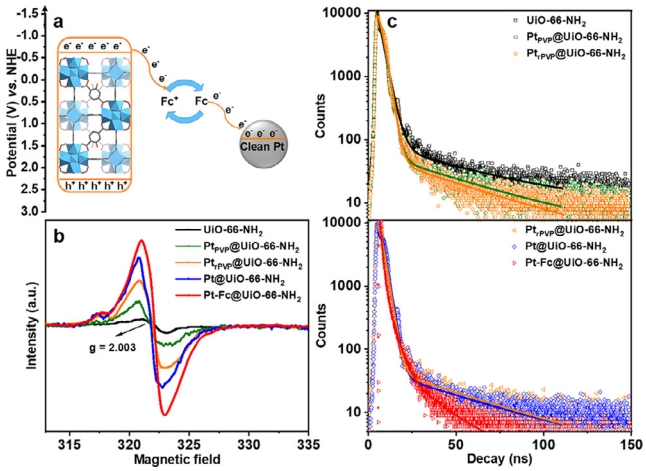

Figure 4. a) Illustration showing electron migration path in the photocatalytic H_2 production of Pt-Fc@UiO-66-NH_2. b) ESR spectra (under visible-light irradiation for 90 s) and c) time-resolved PL spectra ($\lambda_{ex}=380$ nm, $\lambda_{em}=455$ nm) for UiO-66-NH_2, Pt_{PVP}@UiO-66-NH_2, Pt_{rPVP}@UiO-66-NH_2, Pt@UiO-66-NH_2, and Pt-Fc@UiO-66-NH_2.

The aforementioned ESR spectra clearly conclude that Fc behaves as an effective electron relay mediator via the conversion of Fe^{3+}/Fe^{2+} in Pt-Fc@UiO-66-NH_2, as described in Figure 4a. To get further insight into the mechanism behind the tailored photocatalytic H_2 production, ESR in conjunction with time-resolved PL spectroscopy have been conducted to the charge transfer process. All photocatalysts show a strong ESR peak at $g=2.0023$ under illumination, which is ascribed to the oxygen-centered active sites in Zr-oxo clusters generated by link-to-cluster electron transfer (LCCT) (Figure 4b).[16] The ESR signal intensity follows the order of UiO-66-NH_2 < Pt_{PVP}@UiO-66-NH_2 < Pt_{rPVP}@UiO-66-NH_2 < Pt@UiO-66-NH_2 < Pt-Fc@UiO-66-NH_2, in accordance with the trend of electron transfer (Figure 2b–d). The stronger intensity of ESR signal could be attributed to the faster speed of photoinduced electron transfer.[9d] Furthermore, the fitting of time-resolved PL spectra determines the PL lifetimes to be 10.59 ns (UiO-66-NH_2), 2.93 ns (Pt_{PVP}@UiO-66-NH_2), 2.37 ns (Pt_{rPVP}@UiO-66-NH_2), 2.06 ns (Pt@UiO-66-NH_2), and 0.96 ns (Pt-Fc@UiO-66-NH_2), respectively (Figure 4c). The shorter PL lifetime means more effective e-h separation. Getting all above results together, it is unambiguously proved that the removal of PVP and introduction of Fc are able to suppress the e-h recombination and accelerate the sluggish kinetics of electron transfer, leading to enhanced photocatalytic activity.

In summary, the UiO-66-NH_2 incorporating uniform Pt NPs has been adopted as an ideal platform to investigate the influence of interfacial microenvironment modulation (by PVP removal on the Pt) on electron transfer and corresponding photocatalysis. Though similar Pt sizes and loading contents, the MOF encapsulating the Pt capped with PVP, Pt with partially removed PVP, or Pt without interfacial PVP exhibit distinctly different electron transfer kinetics. The surface-clean Pt is favorable for interfacial electron transfer. Accordingly, Pt@UiO-66-NH_2 offers enhanced activity, superior to Pt_{rPVP}@UiO-66-NH_2, followed by Pt_{PVP}@UiO-66-NH_2 and the nearly inactive UiO-66-NH_2, in the photocatalytic H_2 production. Along this way of thinking, electron transfer efficiency is further promoted by introducing an electron mediator of Fc into Pt@UiO-66-NH_2, giving rise to the best activity of Pt-Fc@UiO-66-NH_2. This study, for the first time, not only enables deep insights into the influence of interfacial surfactant between the photosensitizer and cocatalyst on electron transfer kinetics and related activity, but also provides significant inspirations on microenvironment modulation of catalytic centers for photocatalysis.

Acknowledgements

This work was supported by the NSFC (21725101, 22161142001 and 21521001), Dalian National Laboratory Cooperation Fund, CAS (DNL201911), Collaborative Innovation Program of Hefei Science Center, CAS (2020HSC-CIP005).

Conflict of interest

The authors declare no conflict of interest.

Keywords: hydrogen production · interfacial electron transfer · metal–organic frameworks · microenvironment modulation · photocatalysis

[1] a) J. Kim, D. Hansora, P. Sharma, J. Jang, J. Lee, *Chem. Soc. Rev.* **2019**, *48*, 1908–1971; b) Q. Wang, K. Domen, *Chem. Rev.* **2020**, *120*, 919–985.

[2] a) X. Chen, S. Shen, L. Guo, S. Mao, *Chem. Rev.* **2010**, *110*, 6503–6570; b) Z. Wang, C. Li, K. Domen, *Chem. Soc. Rev.* **2019**, *48*, 2109–2125.

[3] a) J. Yang, D. Wang, H. Han, C. Li, *Acc. Chem. Res.* **2013**, *46*, 1900–1909; b) A. Meng, L. Zhang, B. Cheng, J. Yu, *Adv. Mater.* **2019**, *31*, 1807660; c) J. Ran, J. Zhang, J. Yu, M. Jaroniecc, S. Z. Qiao, *Chem. Soc. Rev.* **2014**, *43*, 7787–7812.

[4] a) F.-M. Zhang, J.-L. Sheng, Z.-D. Yang, X.-J. Sun, H.-L. Tang, M. Lu, H. Dong, F.-C. Shen, J. Liu, Y.-Q. Lan, *Angew. Chem. Int. Ed.* **2018**, *57*, 12106–12110; *Angew. Chem.* **2018**, *130*, 12282–12286; b) S. Xie, Y. Wang, Q. Zhang, W. Deng, Y. Wang, *ACS Catal.* **2014**, *4*, 3644–3653; c) G. Zhang, Z.-A. Lan, L. Lin, S. Lin, X. Wang, *Chem. Sci.* **2016**, *7*, 3062–3066; d) X. Fang, Q. Shang, Y. Wang, L. Jiao, T. Yao, Y. Li, Q. Zhang, Y. Luo, H.-L. Jiang, *Adv. Mater.* **2018**, *30*, 1705112; e) H. Liu, H. Song, W. Zhou, X. Meng, J. Ye, *Angew. Chem. Int. Ed.* **2018**, *57*, 16781–16784; *Angew. Chem.* **2018**, *130*, 17023–17026.

[5] a) W.-N. Wang, W.-J. An, B. Ramalingam, S. Mukherjee, D. M. Niedzwiedzki, S. Gangopadhyay, P. Biswas, *J. Am. Chem. Soc.* **2012**, *134*, 11276–11281; b) I. Vamvasakis, B. Liu, G. S. Armatas, *Adv. Funct. Mater.* **2016**, *26*, 8062–8071.

[6] a) M. Luo, W. Yao, C. Huang, Q. Wu, Q. Xu, *J. Mater. Chem. A* **2015**, *3*, 13884; b) J.-D. Xiao, Q. Shang, Y. Xiong, Q. Zhang, Y. Luo, S.-H. Yu, H.-L. Jiang, *Angew. Chem. Int. Ed.* **2016**, *55*, 9389–9393; *Angew. Chem.* **2016**, *128*, 9535–9539; c) L. Jiao, J. Wang, H.-L. Jiang, *Acc. Mater. Res.* **2021**, *2*, 327–339.

[7] a) L. Shang, T. Bian, B. Zhang, D. Zhang, L.-Z. Wu, C.-H. Tung, Y. Yin, T. Zhang, *Angew. Chem. Int. Ed.* **2014**, *53*, 250–254; *Angew. Chem.* **2014**, *126*, 254–258; b) Y.-B. Huang, Q. Wang, J. Liang, X. Wang, R. Cao, *J. Am. Chem. Soc.* **2016**, *138*, 10104–10107; c) Q. Zhu, Q. Xu, *Chem* **2016**, *1*, 220–245; d) H. He, Y.

Cui, B. Li, B. Wang, C. Jin, J. Yu, L. Yao, Y. Yang, B. Chen, G. Qian, *Adv. Mater.* **2019**, *31*, 1806897.

[8] a) S. Zheng, T. Wu, C.-T. Chou, A. Fuhr, P. Feng, X. Bu, *J. Am. Chem. Soc.* **2012**, *134*, 4517 – 4520; b) H. Furukawa, K. E. Cordova, M. O'Keeffe, O. M. Yaghi, *Science* **2013**, *341*, 1230444; c) H.-C. Zhou, S. Kitagawa, *Chem. Soc. Rev.* **2014**, *43*, 5415 – 5418; d) T. Islamoglu, S. Goswami, Z. Li, A. J. Howarth, O. K. Farha, J. T. Hupp, *Acc. Chem. Res.* **2017**, *50*, 805 – 813; e) Q. Yang, Q. Xu, H.-L. Jiang, *Chem. Soc. Rev.* **2017**, *46*, 4774 – 4808; f) H. Li, L. Li, R.-B. Lin, W. Zhou, Z. Zhang, S. Xiang, B. Chen, *EnergyChem* **2019**, *1*, 100006.

[9] a) G. Lu, S. Li, Z. Guo, O. K. Farha, B. G. Hauser, X. Qi, Y. Wang, X. Wang, S. Han, X. Liu, J. S. D. Chene, H. Zhang, Q. Zhang, X. Chen, J. Ma, S. C. J. Loo, W. Wei, Y. Yang, J. T. Hupp, F. Huo, *Nat. Chem.* **2012**, *4*, 310 – 316; b) X. Li, T. W. Goh, L. Li, C. Xiao, Z. Guo, X. Zeng, W. Huang, *ACS Catal.* **2016**, *6*, 3461 – 3468; c) H. Liu, L. Chang, C. Bai, L. Chen, R. Lu, Y. Li, *Angew. Chem. Int. Ed.* **2016**, *55*, 5019 – 5023; *Angew. Chem.* **2016**, *128*, 5103 – 5107; d) J.-D. Xiao, L. Han, J. Luo, S.-H. Yu, H.-L. Jiang, *Angew. Chem. Int. Ed.* **2018**, *57*, 1103 – 1107; *Angew. Chem.* **2018**, *130*, 1115 – 1119; e) G. Li, S. Zhao, Y. Zhang, Z. Tang, *Adv. Mater.* **2018**, *30*, 1800702.

[10] a) Y. Fu, D. Sun, Y. Chen, R. Huang, Z. Ding, X. Fu, Z. Li, *Angew. Chem. Int. Ed.* **2012**, *51*, 3364 – 3367; *Angew. Chem.* **2012**, *124*, 3420 – 3423; b) X. Dong, M. Zhang, R. Pei, Q. Wang, D. Wei, S. Zang, Y. Fan, T. Mak, *Angew. Chem. Int. Ed.* **2016**, *55*, 2073 – 2077; *Angew. Chem.* **2016**, *128*, 2113 – 2117; c) G. Wu, J. Huang, Y. Zang, J. He, G. Xu, *J. Am. Chem. Soc.* **2017**, *139*, 1360 – 1363; d) A. Dhakshinamoorthy, Z. Li, H. García, *Chem. Soc. Rev.* **2018**, *47*, 8134 – 8172; e) J.-D. Xiao, H.-L. Jiang, *Acc. Chem. Res.* **2019**, *52*, 356 – 366; f) J. Ran, J. Qu, J. Zhang, H. Wen, T. Wang, H. Chen, S. Zhang, L. Song, X. Zhang, L. Jing, R. Zheng, S. Z. Qiao, *Adv. Energy Mater.* **2019**, *9*, 1803402; g) Y. Zhang, J. Pang, J. Li, X. Yang, M. Feng, P. Cai, H.-C. Zhou, *Chem. Sci.* **2019**, *10*, 8455 – 8460; h) J. Wang, L. Qiao, H. Nie, H. Huang, Y. Li, S. Yao, M. Liu, Z. Zhang, Z. Kang, T. Lu, *Nat. Commun.* **2021**, *12*, 813.

[11] a) C. Wang, K. deKrafft, W. Lin, *J. Am. Chem. Soc.* **2012**, *134*, 7211 – 7214; b) L. Shen, M. Luo, L. Huang, P. Feng, L. Wu, *Inorg. Chem.* **2015**, *54*, 1191 – 1913; c) T. Zhou, Y. Du, A. Borgna, J. Hong, Y. Wang, J. Han, W. Zhang, R. Xu, *Energy Environ. Sci.* **2013**, *6*, 3229 – 3234; d) S. Yang, D. Fan, B. Pattengale, C. Liu, X. Zhang, J. Huang, *J. Phys. Chem. C* **2018**, *122*, 3305 – 3311.

[12] Y. Zhao, N. Kornienko, Z. Liu, C. Zhu, S. Asahina, T. Kuo, W. Bao, L. Xie, A. Hexemer, O. Terasaki, P. Yang, O. M. Yaghi, *J. Am. Chem. Soc.* **2015**, *137*, 2199 – 2202.

[13] G. He, Y. Song, K. Liu, A. Walter, S. Chen, S. Chen, *ACS Catal.* **2013**, *3*, 831 – 838.

[14] Z. Xue, K. Liu, Q. Liu, Y. Li, M. Li, C.-Y. Su, N. Ogiwara, H. Kobayashi, H. Kitagawa, M. Liu, G. Li, *Nat. Commun.* **2019**, *10*, 5048.

[15] K. Wu, K. Li, S. Chen, Y.-J. Hou, Y.-L. Lu, J.-S. Wang, M.-J. Wei, M. Pan, C.-Y. Su, *Angew. Chem. Int. Ed.* **2020**, *59*, 2639 – 2643; *Angew. Chem.* **2020**, *132*, 2661 – 2665.

[16] H. Liu, C. Xu, D. Li, H.-L. Jiang, *Angew. Chem. Int. Ed.* **2018**, *57*, 5379 – 5383; *Angew. Chem.* **2018**, *130*, 5477 – 5481.

Manuscript received: March 25, 2021
Revised manuscript received: May 5, 2021
Accepted manuscript online: May 14, 2021
Version of record online: June 24, 2021

